

2021

Combined Experimental and Modeling Analysis for the Development of Optical Materials Suitable to Enhance the Implementation of Plasmonic-Enhanced Luminescent Down-Shifting Solutions on Existing Silicon-Based Photovoltaic Devices

James Walshe

Technological University Dublin, james.walshe@tudublin.ie


Mihaela Girtan

Matrix, Université d'Angers

Sarah McCormack

Trinity College Dublin, Ireland

Follow this and additional works at: <https://arrow.tudublin.ie/cieoart>
See next page for additional authors

 Part of the [Optics Commons](#)

Recommended Citation

Walshe, J. et al. (2021) Combined Experimental and Modeling Analysis for the Development of Optical Materials Suitable to Enhance the Implementation of Plasmonic-Enhanced Luminescent Down-Shifting Solutions on Existing Silicon-Based Photovoltaic Devices, *ACS Appl. Electron. Mater.* 2021, 3, 6, 2512–2525 DOI:10.1021/acsaelm.1c00018

This Article is brought to you for free and open access by the Centre for Industrial and Engineering Optics at ARROW@TU Dublin. It has been accepted for inclusion in Articles by an authorized administrator of ARROW@TU Dublin. For more information, please contact arrow.admin@tudublin.ie, aisling.coyne@tudublin.ie.



This work is licensed under a [Creative Commons Attribution-NonCommercial-Share Alike 4.0 License](#)

Authors

James Walshe, Mihaela Girtan, Sarah McCormack, John Doran, and George Amarandei

Combined Experimental and Modeling Analysis for the Development of Optical Materials Suitable to Enhance the Implementation of Plasmonic-Enhanced Luminescent Down-Shifting Solutions on Existing Silicon-Based Photovoltaic Devices

James Walshe,* Mihaela Girtan, Sarah McCormack, John Doran, and George Amaranidei



Cite This: *ACS Appl. Electron. Mater.* 2021, 3, 2512–2525



Read Online

ACCESS |



Metrics & More



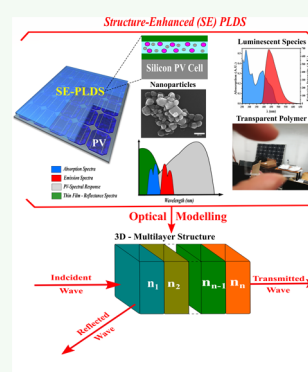
Article Recommendations



Supporting Information

ABSTRACT: The development of highly efficient solar collectors requires modulating the light interactions with the semiconducting materials. Incorporating luminescent species and metal nanoparticles within a semitransparent polymeric material (e.g., polymethyl methacrylate (PMMA)) leads to the formation of a plasmon-enhanced luminescent down-shifting (PLDS) layer, which offers a retrofittable approach toward expanding the wavelength range over which the conversion process can effectively occur. Adding antireflection coatings (ARCs) further controls the spectral response. However, with each additional component comes additional loss pathways. In this study, the losses related to light interactions with the PMMA and the ARCs have been investigated theoretically using a transfer matrix method and experimentally validated. Two proposed architectures were considered, and the deviations between the optical response of each iteration helped to establish the design considerations. The proposed structure-enhanced (SE) designs generated a predicted enhancement of 37 to 62% for the collection performance of a pristine monocrystalline-silicon solar cell, as inferred through the short-circuit current density (J_{sc}). The results revealed the synergies among the SE-design components, demonstrating that the spectral response of the SEs, containing a thin polymer framework and an ARC, can be tuned to minimize the reflections, leading to the solar energy conversion enhancement.

KEYWORDS: spectral conversion, light management, plasmonics, silicon solar cells, optical modeling, thin films, luminescent down-shifting, plasmonic luminescent down-shifting



1. INTRODUCTION

In the efforts to modularize photovoltaic (PV) cells into large-scale industrial panels, a series of polymeric and glass layers are integrated into the panel architecture to provide a protective shield from the harsh environmental conditions (temperature, humidity, etc.).¹ The encapsulating materials, typically a combination of polymethyl methacrylate (PMMA) and/or tempered glass derivatives, impinge upon the conversion dynamics of the underlying PV technology.^{2–4} Consequently, the addition of the encapsulants has a great influence on the spectral response⁵ and short-circuit current density⁶ generated within a PV device, particularly within the ultraviolet region (300–400 nm), where PMMA exhibits a sharp spectral cutoff.⁸ To counteract these additional losses, the fundamental architecture of the photoconductive material is drastically altered through surface passivation, surface texturing, or by tailoring the material band gap dynamics through selectively doping the crystal lattice.^{1,4,9,10} However, for each additional processing stage implemented into the device design, the fabrication costs grow.^{11,12} To continue the reductions experienced in PV pricing,^{11–13} alongside with the continuous improvement of the conversion efficiencies,^{11–13} various

alternative intricate architectures have been suggested.^{4,9} As the complexity of the PV architecture continues to grow, optical modeling starts to become the preferred tool to resolve and decouple the complex physical phenomena affecting the energy harvesting. Often, the optical modeling is used for the stratified structures to find the optimum configuration allowing them to maximize their energy harvesting potential.^{2,3,14,15}

Plasmon-enhanced luminescent down-shifting (PLDS) is an experimental approach that could improve the narrow spectral responsivity of PV technology through the incorporation of adaptive materials. In this alternative approach, no alteration of the intrinsic properties of the semiconducting material is required to enhance the spectral properties of the PV conversion process.^{16–19} In this strategy, the PLDS layer captures solar energy from the targeted spectral region, where

Received: January 6, 2021

Accepted: May 13, 2021

Published: May 26, 2021



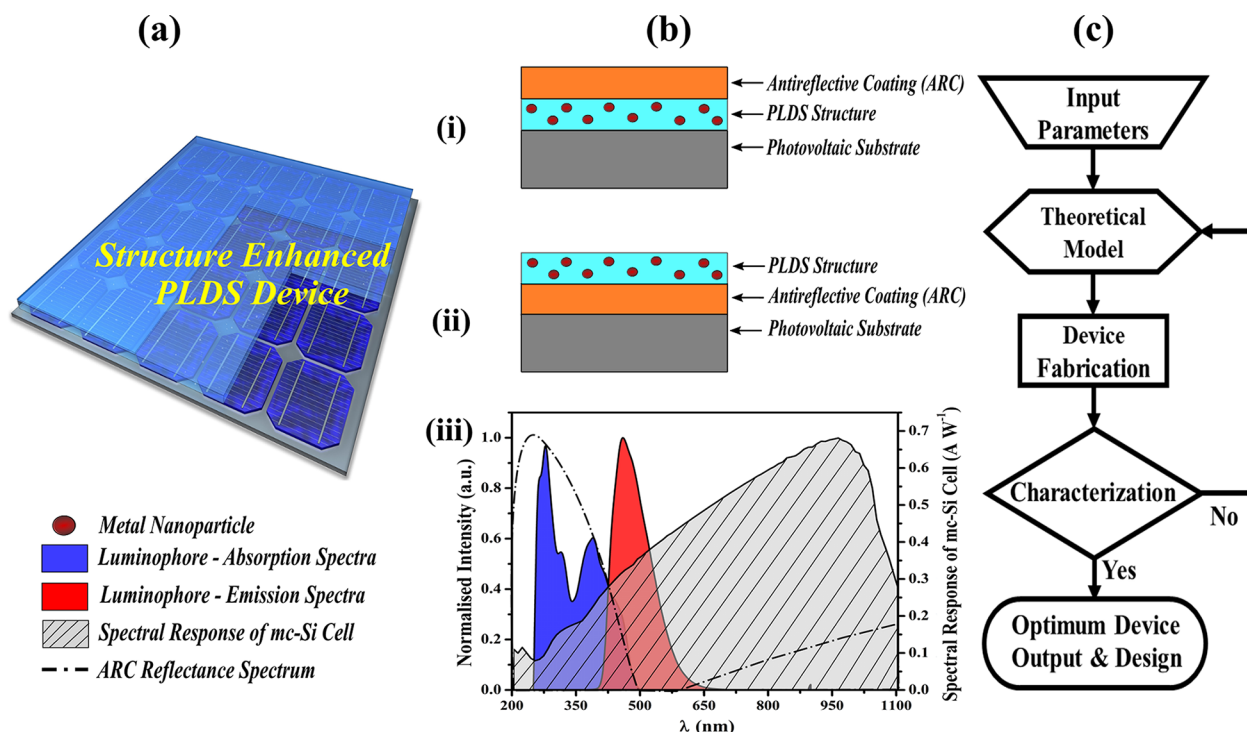


Figure 1. (a) Schematic of the structure-enhanced plasmonic luminescent down-shifting (SE-PLDS) on top of the photovoltaic device. (b) The two SE-PLDS architectures (i,ii) assessed and (iii) the spectral working principle of this type of device. The structural elements reflection profile (b.iii—dashed black line) is customized to lead to a maximum intensity within the absorption window of the photoluminescent material employed (b.iii—blue). At the same time, it will reduce the reflectivity across the photoluminescent material (luminophores) emission range (b.iii—red) and the high spectral responsivity window (b.iii—gray-filled area) of the photovoltaic technology (in this case, mc-Si PV). (c) The schematic overview of the steps performed to evaluate the properties and overall performance of the SE-PLDS structures to optimize the design of SE-PLDS devices, where the PLDS layer was replaced by a pristine PMMA framework (i.e., containing no luminophores or MNPs).

the PV cell sustains “poor” spectral conversion performances (295–500 nm) due to its fixed band gap energy and the unwanted associated thermal processes (“thermalization losses”) that follow.^{20,61} The captured solar irradiance is subsequently down-shifted and re-emitted via the process of plasmon-assisted photoluminescence at higher frequencies. This minimizes the spectral mismatch that exists between the spectral responsivity of the PV cell and the energy distribution throughout the solar spectrum. Consequently, more photons are capable of impinging the PV cell at an energy that more closely matches the band gap of the PV material, and thus, a larger photocurrent is produced.^{20,61}

Replacing the inactive encapsulating material with a (semi)transparent framework (Figure 1), doped with selectively absorbing species that modulate the solar spectrum, improves the losses stemming from the parasitic absorption exhibited by PMMA or other encapsulating materials.^{3,15} Through the addition of metal nanoparticles (MNPs) within the encapsulating layer, a higher degree of control and promotion of the photoluminescent behavior of the embedded luminescent material can be achieved.²¹ Thus, the strong electromagnetic fields are formed on the surface of the MNPs. These fields not only can alter the photoluminescent properties of the polymer but also advantageously attune the physical properties of the nanocomposite encapsulant.^{22–25} However, the nonideal optical properties exhibited by most encapsulating materials (e.g., a typical refractive index $n \approx 1.4–1.6$), in combination with the myriad of additional loss mechanisms introduced through the presence of the luminescent material

and MNPs, require further improvement from the classical PLDS approach.

Typically, the influence of each PLDS iteration on the solar energy conversion abilities of a PV cell are experimentally determined through a successive series of trial and error.^{3,15} This implies fitting each combination of encapsulant, luminescent material, and MNP directly onto a PV structure and recording the difference in the acquired performance.^{3,15} In this context, the enhancements resolved in the PV device performance are including the contributions stemming solely from the optical properties of the materials as well as the contributions that arise as a consequence of the modulation of the incoming solar irradiance through plasmon-assisted photoluminescence. Consequently, the extent to which each one of these contributions imparts the electrical conversion efficiency of the PV architecture has been typically overlooked in the pursuit of examining their combined influence.^{6,7} However, by decoupling the various optical interactions and investigating their individual influence on the optical behavior and corresponding conversion performance of PV devices, the premises to further optimize any collaborative and complementary interactions that may arise among the individual elements (PV structure, encapsulant, luminophore, MNPs) can be offered.⁷ Various modeling approaches allowing the influence of the PLDS layer optical properties on the electrical characteristics of a pristine PV have been developed over the years to explore the interactions that can occur within these complex optical structures.^{7,26–28} These approaches are using either wave-based optical relationships or more probabilistic photon-based methods to allow them to calculate the

fundamental properties and the performances of the modeled optical system.^{26–29} The PLDS approaches, in conjunction with the capability of antireflective coatings (ARCs) to suppress the optical reflection losses arising from the front surface of a device and/or act as wavelength-selective highly reflective surfaces, offer further means of alleviating the additional losses introduced through the PLDS layer.^{7,30,31} However, the presence and the functionality of the PLDS devices relies upon the existence of a series of synergies between the luminophore and the antireflective coatings. Thus, the optical properties produced by the complex configuration of encapsulating frameworks and ARCs, in general, can help or hamper the benefit of having the luminophore and the MNPs embedded in the host polymer matrix. Therefore, it is essential to first investigate and establish the impact of the host polymer on the resulting spectral properties, *prior* to the addition of the different other species (e.g., luminophores, nanoparticles, etc.) or thin films, which will modulate the solar irradiance via PLDS. Under this scenario, the conversion efficiency of the solar collection system can be maximized as each new element will be introduced in the design. For an appropriate understanding of the behavior of these complex designs, a combination of theoretical and experimental approaches is required.

Here, the impact of simple single-layer ARCs and of a polymer-encapsulating layer on the optical and electrical properties of a pristine monocrystalline-silicon (mc-Si) PV was experimentally investigated and theoretically modeled using a generalized transfer-matrix-based method. For the structures examined, optical materials that are frequently implemented as highly transparent (thin-film) ARCs were used. Through the successive experimental fabrication and optical characterization of different polymeric-encapsulated and thin-film structures, the outputs generated by the model were correlated to performances achieved under laboratory conditions. This enabled for the divergences between the expected (modeled) behavior and the actual (measured) behavior of the devices to be quantified, resolved, and utilized to recalibrate the performance metrics employed in the modeling environment. The ARCs' ability to modulate the optical interactions was investigated and optimized prior to their insertion in the proposed structure-enhanced (SE) devices. The influence of each design component (PMMA layer, thin-film (i.e., ARC)) on the overall performance of the SE-device was explored by developing and characterizing, experimentally and theoretically, two possible designs of the SE-device. The influence of the coatings' composition, configuration, and optical thickness on affecting the conversion efficiency of the PV system was investigated to maximize the amount of "clean" electricity that was produced in the SE configuration. The differences among the conversion efficiencies obtained by adding purely an ARC, the PMMA encapsulant, and the SE-designs were surveyed using the calibrated model. Finally, the study establishes the framework for the initial design requirements for passive SE-devices, which can offer a solution in enhancing the PV cells' efficiencies. Such SE-devices could lead to efficiency values, which can be beyond those achieved when conventional PLDS approaches are used.

1.1. Structure-Enhanced Devices. In the process of integrating an LDS layer onto a PV collection system, a cascade of additional optical pathways is created within the encapsulated PV structures.¹⁴ Through the cumulative

influence of the layer's spectral properties, optical thickness, and LDS properties, the energy transmitted into the coupled PV cell can be either increased, or alternatively, the energy losses can become intensified. This leads to the requirement for further revisions in the PV assembly design. The primary mechanism that is responsible for promoting the dominance of an overall negative enhancement in the conversion performance of an LDS-fitted PV device originates in the nonideal optical properties of the photoluminescent materials currently available. The material limitations can be further compounded by the fact that most encapsulating materials employed in LDS applications exhibit some degree of susceptibility to photo-irradiation and/or absorb irradiation from within the spectral range targeted by the LDS species.^{3,7,15} Moreover, the low refractive index ($n = 1.2–1.6$) of the encapsulating materials typically used until now in manufacturing the LDS devices leads to additional reflection losses, which are occurring at the air–PLDS and PLDS–PV interfaces.^{3,15} These supplementary reflection losses are also introduced by the mismatch between the antireflection coating (e.g., the textured surface or a panoply of thin films aiming to maximize the solar energy collector abilities) formerly integrated into PV architectures and the PLDS layer added.^{32,33} These loss mechanisms does not take into account the control offered over the nanomaterials (e.g., metal nanoparticle) utilized in PLDS devices, which could be used to improve the optical characteristics of the photoluminescent material.^{7,21}

The incorporation into the PLDS architecture of additional optical structures (e.g., simple ARCs as in Figure 1a) could alleviate some of these loss mechanisms.^{30,31} The structure-enhanced PLDS (SE-PLDS) architecture offers the possibility to decrease the reflection losses that arise due to the significant difference between the refractive index of the commonly used encapsulants (e.g., polymers) and the underlying substrate. The ARC design and, consequently, the optical properties of the SE-PLDS structure (see Figure 1b.i,ii) can be tuned to maximize the reflectivity close to the absorption peak of the photoluminescent materials (Figure 1b.iii—blue).

Thereby, this can allow for the potential recycling of the photons that did not previously undergo photoluminescence (Figure 1b.iii). In addition, restraining the structure's reflectivity along the region where the responsivity window of the PV collection system (Figure 1b.iii—gray) is the highest will ensure that most of the photons within this spectral range that are reaching the device will lead to the production of photogenerated charge carriers. Combining these structures with metal (e.g., silver or gold) nanoparticles embedded within the host polymer can lead to a design that is able to compensate for the loss mechanisms that occurred by adding the PLDS/LDS layer.⁷ Moreover, they could offer the possibility of increasing the longevity of such retrofitted devices.³⁴ To understand the implications of adding each new optical element into such a complex stratified SE-PLDS device, the number of design considerations must be reduced accordingly. In this context, this paper will examine only the synergies that are established between the host polymeric matrix (in this case PMMA) and the ARC's presence and how they affect the spectral properties of the device and the efficiency of the PV cell.

2. EXPERIMENTAL AND MODELING METHODS

2.1. Modeling the SE-Devices. In this study, the architecture of the solar cell assembly investigated two layers, an optically thick

polymer layer (10–100 μm) and a thin-film ARC component (20–200 nm) as presented in Figure 1b. The ARC component can be located directly on top of the PLDS (Figure 1b.i), or it can be inserted between the substrate (Figure 1b.ii) and the down-shifting layer (see also ref 7). The down-shifting layer (which, typically, is homogeneously doped with a luminescent material and/or MNP) was modeled as a pristine PMMA film.⁷ In this scenario, the scattering and the absorption contributions from the MNPs (and the luminophore) are not considered in the modeling environment. However, the inclusion of these optical interactions, and their subsequent effect on the deviations inserted in the modified refractive index of the polymeric encapsulant PMMA, has been shown to increase the energy harvesting potential of similar stratified structures, under concentration-dependent conditions.⁷ Therefore, to enable the possible synergies that can exist between the polymer (here, PMMA) and the various ARCs to be resolved and quantified, these interactions were not considered in the optical model. This approach also allows for the remaining optical elements (luminophore and MNPs) to be introduced in a systematic manner at a later stage; however, such considerations are not within the scope of the present work. Consequently, in the model, the SE-devices are effectively simulated as a PMMA (nonfluorescent)-coated PV architecture, which integrates a single-layer ARC either above or below the PMMA layer (Figure 1b.i,ii). During the design process, a wide range of materials were inserted into single-layer ARC components within the SE-device. Thus, materials such as zinc oxide (ZnO), aluminum zinc oxide (Al-ZnO), titanium dioxide (TiO₂), and indium tin oxide (ITO) were investigated. A complete description of the refractive index of the optical materials and their extinction coefficients are presented in the section 1 of the Supporting Information.

In the modeling approach, the multilayered structure is considered to have isotropic optical properties, and the input parameters for each material were the refractive index (n), extinction coefficient (k), and optical thickness (d).⁷ A generalized transfer matrix model (TMM) was implemented to determine the reflectance and transmittance spectra with the detailed description of the model being presented in refs 35 and 7. Monocrystalline silicon (mc-Si) was chosen as the photovoltaic substrate for the SE-devices, and the spectral response was experimentally measured, the solar energy conversion performance of the SE-PLDS devices being assessed under a AM1.5G solar spectrum³⁵ (for further details, see ref 7).

2.2. Optimizing of the Influence of the ARC. An optimization process was developed for the ARC component; its full description being presented in ref 7. Typically, an effective ARC will minimize the structure's overall reflectance within the visible spectral region, where the PV cells are highly efficient.^{3,7,36–39} The electrical contributions resulting from the light conversion can be wavelength-dependent—Figure 1b.iii.⁷ Therefore, the internal quantum efficiency (IQE) of the PV must be considered during the design step.⁴⁰ For practical applications,⁴¹ (see ref 7) the computable effective weighted average reflectance (R_e) metric (eq 1) is more convenient to be used in studies similar to the one considered here^{7,39,41}

$$R_e = \frac{\int_{\lambda_1}^{\lambda_2} I(\lambda) \cdot R(\lambda) \cdot d\lambda}{\int_{\lambda_1}^{\lambda_2} I(\lambda) \cdot d\lambda} \quad (1)$$

where $I(\lambda)$ is the spectral irradiance from the AM1.5G spectrum,³⁶ and $R(\lambda)$ is the structure reflectivity at the given wavelength;⁴¹ λ_2 and λ_1 are the upper and lower limits of the spectral response, respectively. For mc-Si PV cells like those used in this study, the spectral response is 300–1100 nm.^{7,20}

2.3. Current Density Enhancement. To evaluate the effect of each design iteration on the conversion efficiency, the spectral irradiance characteristics should also be considered during the optimization process.^{7,42,43} Optimizing the antireflective element design requires the photocurrent produced under the AM1.5G spectrum to be maximized.^{7,40,44,45} Assuming that other electrical parameters of the PV cell remain unchanged during the optimization of the ARC's structure, the changes in photogenerated current are

well-reflected by the short-circuit current density (J_{sc}).⁷ These assumptions are supported by other experimental studies on ARCs examined on both encapsulated (additional air/glass interface) and nonencapsulated monocrystalline-silicon (mc-Si) solar cells.^{7,40} Thus, while J_{sc} increased even by 25%, the open circuit voltage remained relatively constant ($\sim 2\%$ increase being seen).^{7,49,46} The deviations introduced into the J_{sc} under the design iterations considered can be directly correlated to variations in the electrical power of the mc-Si cell.⁵⁹ Therefore, here, only on the variation within J_{sc} given by eq 2^{7,40,46} will be considered

$$J_{sc} = \int_{\lambda_1}^{\lambda_2} T(\lambda) \cdot \Phi(\lambda) \cdot SR(\lambda) \cdot d\lambda \quad (2)$$

where $\Phi(\lambda)$ is the photon flux under the AM1.5G spectrum, and $SR(\lambda)$ is the spectral response of the photovoltaic material. Eq 2 permits to connect the reflectivity $R(\lambda)$ and absorption $A(\lambda)$ characteristics and the overall device's electrical performance.^{7,40,44} Consequently, the J_{sc} enhancement (%) generated by the antireflective structure addition can be estimated using eq 3⁷

$$J_{sc} \text{ enhancement} = \left(\frac{J_{sc}(\text{device}) - J_{sc}(\text{pristine})}{J_{sc}(\text{pristine})} \right) \quad (3)$$

where J_{sc} (device) is the short-circuit current density delivered using an SE architecture, and J_{sc} (pristine) represents the short-circuit current density of the unaltered pristine (i.e., as received from the manufacturer) mc-Si PV cell.⁷

2.4. Model Validation. An overview of the model validation process (which contained modeling and experimental components) is provided in Figure 1c. This overview highlights the individual aspects of the evaluation process used to optimize the design of the SE-device. The output generated from the transfer matrix model (theoretical model—Figure 1c) can be classified to operate via two distinct predictive pathways: (1) the determination of the structure's reflection spectrum and (2) the enhancement in the J_{sc} achieved through the subsequent fitting of the structure onto the PV substrate. Each mechanism was independently investigated through the deposition and subsequent optical and electrical characterization of single-layer ARCs comprised of ZnO, Al-ZnO, ITO, and TiO₂ deposited across two different substrate materials (commercial mc-Si PV cell, untreated Si wafer). The resulting structures' reflection spectra were characterized using the methodology outlined in Section 2.4.2 to ensure that the reflection properties of the material library considered (inputs—Figure 1c) were accurately represented within the modeling environment. This validation ensured that any insights into the correlation between the reflection suppressive behavior of the ARC (incorporated into the SE-device designs) and the improvements reported reflected a true enhancement in device performance. The conversion performance aspect (characterization—Figure 1c) of the validation process was facilitated through the adoption of relatively inexpensive substrates for the layer deposition, namely an untreated silicon wafer (“control” sample). The “control” sample was subjected to the same specific deposition parameters utilized to coat the commercial grade mc-Si cells (Big Sun Community Solar, San Antonio, Texas, USA) employed in the comparison of the model's efficiency enhancement metric. The reflection spectra, generated using the model, were based upon the thickness values derived from measurements made using ellipsometry (Horiba Jobin Yvon Universal ellipsometer with accompanying Delta Psi software suite) and stylus profilometry (Veeco Dektak 6M, Veeco Instruments Inc., USA). This information (see Figure S2) along with a brief discussion of the importance of accurately representing the materials utilized in the modeled architectures is provided in the Supporting Information. The spectral features, observed in the reflectance spectra registered, were compared with those produced by the model, until both spectra (the measured spectra and the simulated spectra) were in agreement within the confines of statistical significance. The operational ARC-fitted mc-Si devices were characterized experimentally using the setup and protocol outlined in Section 2.4.3 with the order of merit dictated

by a comparison of the simulated evaluation of the structure's performance and its performance under experimental conditions.

2.4.1. Sample Preparation. The PMMA-coated devices were fabricated using spin coating. For a typical preparation procedure, a 50:50 weight percentage solution of the polymer resin (PLEXIT 55 RÖHM—Carl Roth Ltd., Karlsruhe, Germany) was mixed with high-purity pristine dimethyl sulfoxide to form the solution for casting the encapsulant. The resulting solution was vigorously agitated via magnetic stirring at 400–600 rpm for 1 h under ambient conditions to ensure that the solvent was homogeneously dispersed throughout the resin and that no trapped air remained, prior casting the material for spin coating. Consecutively, using a syringe, 1 mL of the solution was displaced at the center of a stationary mc-Si cell (Big Sun Community Solar, San Antonio, Texas, USA), which was secured into the housing of a G3-P8 spin coater (Specialty Coating Systems Inc., Indianapolis, USA) and then subjected to a spin speed of 4000 rpm for 180 s—allowing 10 s for the spin-up and spin-down process. The resulting devices were placed onto a hot plate at 50 °C for 30 min to initiate the annealing process. This initial annealing stage served to remove the inherent stress built up in the PMMA layer throughout the spinning process and improve its optical transparency. In addition, a second annealing stage was employed to further ensure that any remaining solvent or stresses that had been introduced into the polymeric network were minimized or completely removed prior to characterization. In this second annealing stage, the devices were placed inside a Gallenkamp (Gallenkamp & Co. Ltd., Birmingham, United Kingdom) vacuum oven set to a pressure of 100 mbar and temperature of 25 °C for 24 h. This series of steps was repeated for the different substrate materials utilized throughout this study.

The thin films acting as ARC's were sputtered under identical conditions on mc-Si cells and on the control sample. In particular, the samples were positioned in a sputtering system with a vertical target–substrate configuration, the target–substrate distance being ~ 70 mm. The samples were secured onto a rotating disk kept at room temperature. Prior to deposition, the control samples were cleaned with deionized water and ethanol in an ultrasonic bath for 15 min. Mask-sputtering was used to cover a small area (10×10 mm) of the mc-Si (see Figure S3a) and of the control sample (see Figure S3b) during the deposition. The sputtering depositions were made in a reactive atmosphere using In/Sn (90%:10%), Zn, and Ti targets (Kurt Lesker). The deposition rates used during the deposition were 13 nm/min for ITO films ($p = 9 \times 10^{-3}$ mbar, $I = 30$ mA), 23 nm/min for ZnO films ($p = 9 \times 10^{-3}$ mbar, $I = 100$ mA), and 4.8 nm/min for TiO₂ ($p = 9 \times 10^{-3}$ mbar, $I = 100$ mA). After the depositions, the film thicknesses were measured using profilometry and ellipsometry and used to validate the model as previously mentioned.

2.4.2. Reflection Measurement. Reflection measurements were carried out using the reflection spectroscopy setup that is outlined in Figure S4. The reflectance spectra measured served as a comparative to ensure the accuracy and reliability of the spectra derived through the transfer matrix model. Light generated by an Ocean Optics deuterium–hydrogen (DH-2000-BAL) lamp, coupled via a high-sensitivity 600 μ m thick reflectance probe, provided the illumination for the sample. The sample was housed within the Ocean Optics RPH-1 reflectance holder, with all of the measurements carried out under normal incidence. The light reflected from the sample was coupled into an Ocean Optics Flame UV/vis/NIR miniature spectrometer via an accompanying connection provided by the reflectance probe. The system was calibrated using a diffuse reflectance standard WS-1 (Ocean Optics). A series of independent measurements (~ 10 – 15) were performed across each sample surface to check and ensure that any variability in the sample thickness and/or in the uniformity of the fluorophore dispersed throughout was accurately reflected in the spectra acquired.

2.4.3. Current–Voltage (I – V) Characterization. The fundamental solar cell characterization technique is the measurement of the cell's efficiency under the standardized ASTM E1021-15 test conditions.³⁶ Considering the strenuous control required by a system to achieve and maintain these operating conditions, most measurements are carried out under custom-made test rigs (Figure 2) that approximate

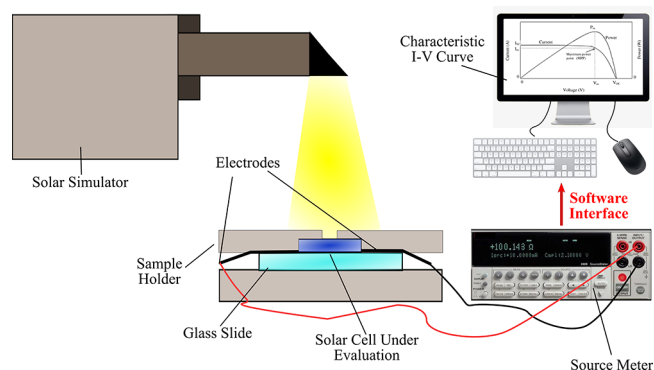


Figure 2. Schematic of the setup used to perform the characteristic current–voltage (I – V) measurement with all of the key components highlighted.

these standardized conditions.^{47,48} The efficiencies reported utilizing such a setup served to form an intercomparison between the cells characterized under the exact same conditions (irradiance, intensity, temperature, and beam size). In this manner, the conversion efficiencies of alternative cell designs, including PMMA and/or ARC-fitted devices, were compared to the unmodified pristine cell's performance. The technique involved evaluating the junction's performance and quality under artificial loading conditions through alteration of the potential applied across the cell. Monitoring the resulting photocurrent generated within the cell, through the implementation of a suitable source meter, such as that shown in Figure 2, enables the cells distinctive I – V response curve to be measured. The performance metrics commonly used to convey the quality of a cell including maximum power, fill factor, and overall efficiency are derived from this curve.⁴⁹

For a typical measurement, devices' (i.e., pristine or PMMA and/or ARC-fitted devices) 2×2 cm monocrystalline-silicon solar cells (Big Sun Community Solar, San Antonio, Texas, USA) were used. The cells were fitted onto glass substrates in order to ensure they remained completely flat throughout the measurement. The substrates were then carefully placed within a sample holder (shown in Figure 2), which further secured the devices throughout the measurement while also ensuring that the aperture diameter of the incident beam was maintained at 10 mm throughout the measurement. Consequently, only the signal collected from an area of 10×10 mm contributed toward the recorded electrical values. In addition, to mitigate the influence of the irradiated area being reduced through the presence of busbars and the local fluctuations in conversion performance experienced across the surface area of the PV devices, each measurement was independently repeated three times.

For each measurement, the substrate was secured in the sample holder by ensuring that a similar set of busbars (see Figure S3a) remained parallel to the periphery of the aperture. Similar size areas were used to measure the response of thin film coated and uncoated (i.e., pristine) mc-Si cell (see Figure S3a). This alignment was considered for each successive measurement of the area of the cell that was exposed. Different points on the cell's surface were investigated to account for the localized fluctuations in the crystal properties. The results presented here represent an average of these measurements. A Keithley 2400 source meter (Keithley Instruments, Cleveland, Ohio, USA) was used to perform the measurements, with the resulting I – V curve generated through a LabVIEW interface.

3. RESULTS AND DISCUSSIONS

3.1. Modulating the Reflection Suppression Capabilities of Simple Antireflection Elements. Before the optical and electrical behavior of the SE PV systems could be accurately modeled, it was first necessary to demonstrate the behavior of each individual design component (PV cell, polymeric encapsulant layer, and the antireflective coating)

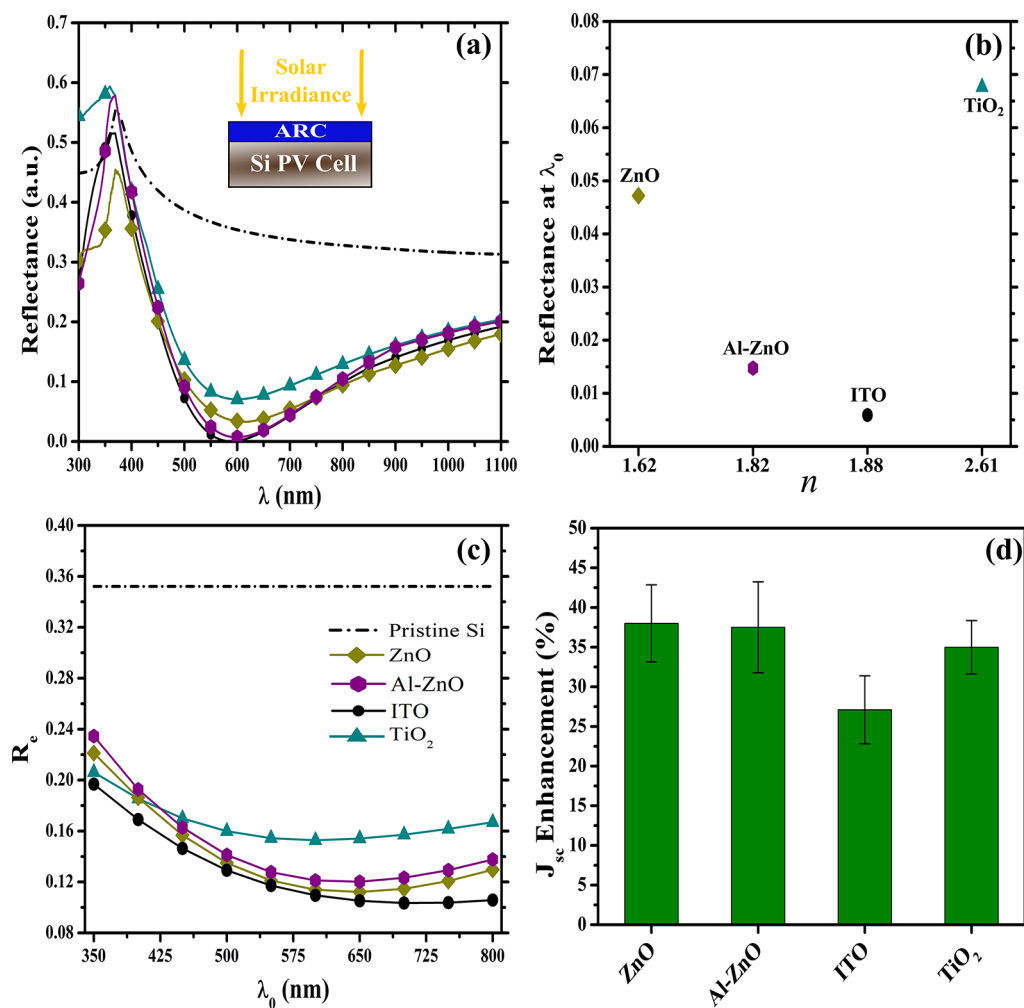


Figure 3. (a) The reflection spectra as generated using the computational model for different single-layer ARCs, which were designed to perform as a $\lambda/4$ film at $\lambda_0 = 600$ nm, and (b) the change in the reflectance at $\lambda_0 = 600$ nm for materials with various refractive indexes (n). The ideal ARC material is emphasized. (c) The effective weighted average reflectance (R_c) as determined by the variation in ARC thickness at λ_0 . (d) The predicted J_{sc} enhancement for each ARC placed onto a pristine mc-Si PV cell. The error bars represent the enhancement deviation obtained using different values of material thickness. The legend for the entire figure is presented in figure (c).

within the overarching composite device (characterization stage in Figure 1c). The evaluation process was broken down into three distinctive aspects: (1) the assessment of the optical tunability offered through single-layer ARCs and their subsequent impact on the electrical performance of the PV cell, (2) the verification of the model's predictive capabilities when describing the optical and electrical behavior of the various materials encountered throughout this study, and (3) the determination of the possible enhancement in the conversion efficiency achievable with the SE-device designs considered and developed herein.

3.1.1. Optical Behavior of Single-Layer ARCs. Silicon (Si) in its pristine and untreated form endures a substantial 35–40% loss in light-collection efficiency (Figure 3a, broken black line) over the spectral region where the semiconducting material exhibits peak conversion efficiencies, i.e., the 450–1100 nm spectral bandwidth. An intensified reflection loss of 55–60% (Figure 3a, broken black line) arises over the ultraviolet spectral region (300–400 nm) and stems from silicon's considerably high refractive index within the narrowband of frequencies,⁵⁰ and thus, it dominates the total losses of the untreated PV device. Figure 3a also highlights the

ability of single-layer ARCs composed of common optical materials to suppress the reflection losses arising from the front surface of the PV device.

It can be observed from Figure 3a that selecting even a single-layer ARC to be included in the SE-designs facilitates the suppression of reflections over a relatively large (250–300 nm) spectral bandwidth. Furthermore, through the subtle modification of the thin-films' optical thickness, this spectral bandwidth can be controlled. The optical thickness of an ARC is typically expressed as the wavelength (λ_0) at which the film(s) are designed to perform as a quarter-wavelength thick optical medium,³⁵ and it is calculated using the optical materials refractive index (n) at the given wavelength.³⁵

Additionally, Figure 3a highlights that irrespective of the ARC's optical properties, the reflectance of the PV device becomes dramatically diminished, especially within the 450–1100 nm spectral window. Adapting the optical thickness of the ARC to 600 nm enabled the highest performance to be elicited from the PV material. This behavior derives from the combination of the spectral distribution of the irradiance within the solar spectrum and the spectral responsivity of the mc-Si substrate, the product of which is maximized at the

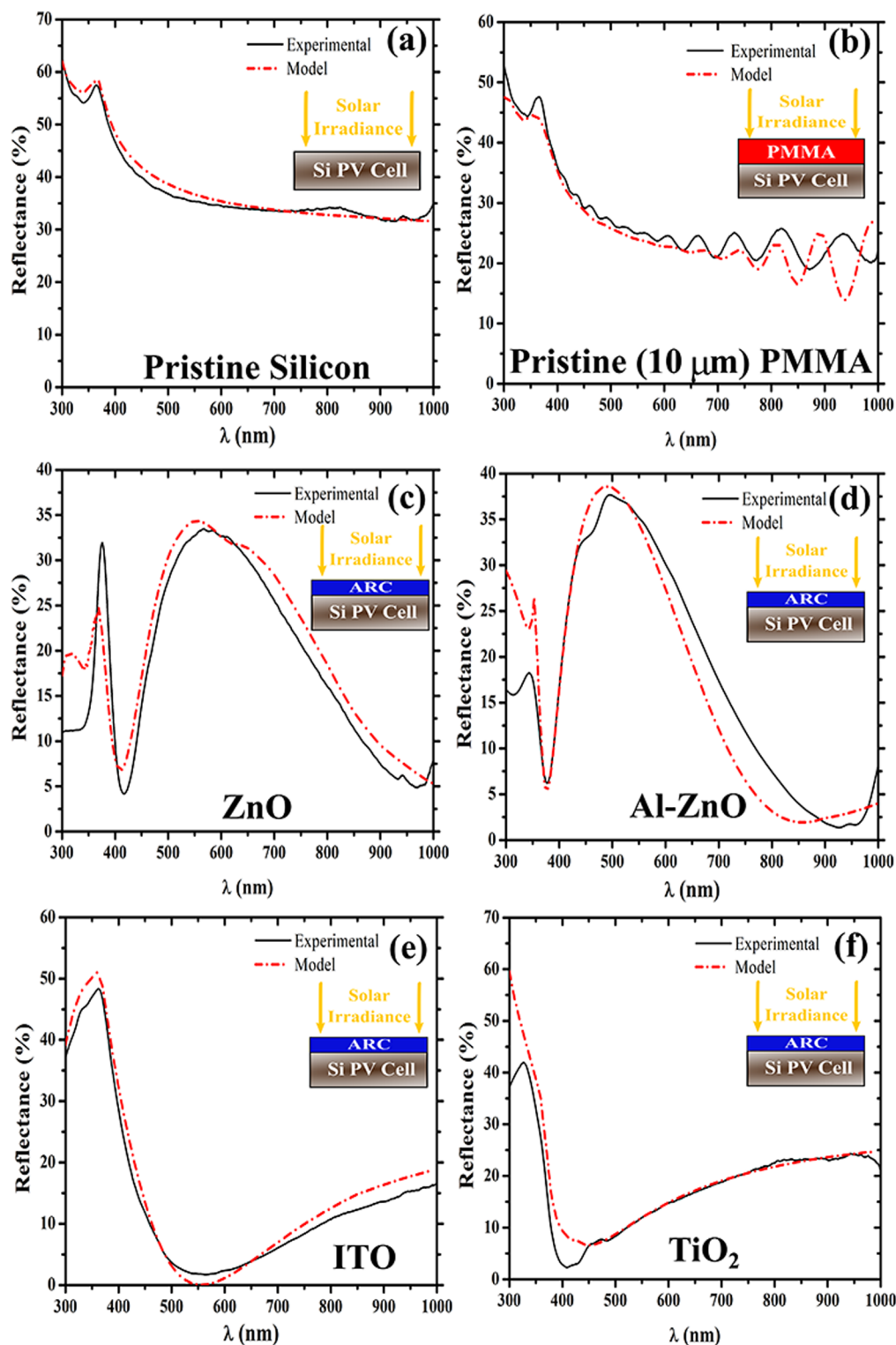


Figure 4. Comparison between the reflectance spectra derived using the transfer matrix model (broken red line) and the reflectance spectra determined experimentally (black solid line) for a number of different types of material: (a) pristine untreated silicon, (b) pristine 10 μm thick polymethyl methacrylate, also known as PMMA, (c) zinc oxide (ZnO), (d) aluminum zinc oxide (Al-ZnO), (e) indium tin oxide (ITO), and (f) titanium dioxide (TiO_2). A schematic of each structure is included in the insets.

central band of frequencies surrounding this wavelength. Furthermore, by monitoring the influence of the variation of the refractive index of the ARC material onto the changes in the reflectance at a fixed wavelength of 600 nm (Figure 3b), the enhancement and the subsequent need for optimization of the coating through the careful selection of the optical material

becomes clear. For single-layer ARCs, this translates to an ideal refractive index of ~ 1.97 , which is closely matched by an indium tin oxide (ITO) layer. Moreover, they must also accommodate a favorable combination of chemical, physical, and mechanical attributes.⁵¹

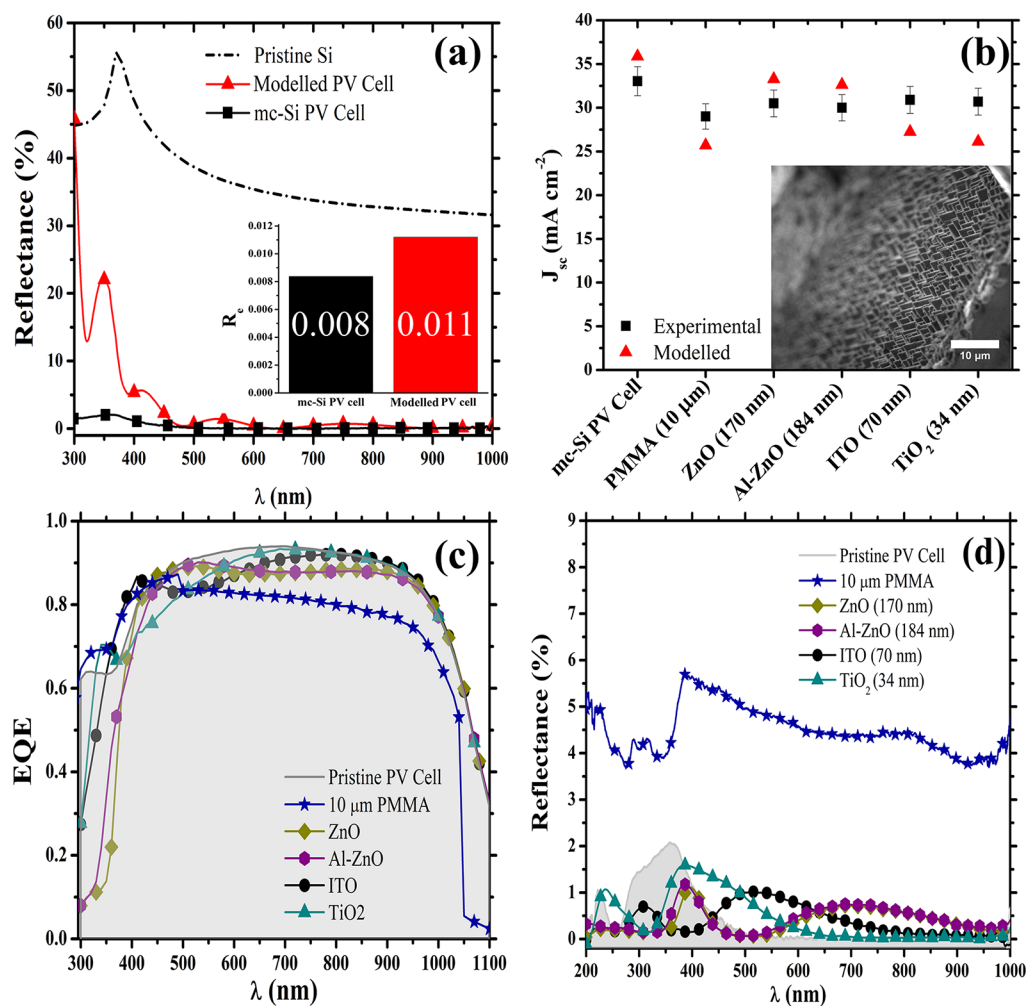


Figure 5. (a) The divergence in the reflectance spectrum exhibited by untreated pristine silicon (pristine Si, broken black line), a commercial high-grade monocrystalline-silicon photovoltaic cell (mc-Si PV cell, black squares), and a similar antireflective-fitted mc-Si device designed to replicate the optical and electrical behavior of the commercial PV cell (modeled PV cell, red triangles). A direct comparison between the effective weighted average reflectance (R_c) of the commercial PV cell and the modeled PV device is additionally provided in the inset. (b) The short-circuit current density (J_{sc}) of the physical devices fabricated and measured experimentally (black squares) and the corresponding behavior of the imitated device (red triangles) when fitted with the same series of antireflection coatings (ARCs). A scanning electron microscope (SEM) image of the mc-Si PV cell front surface is provided in the inset. (c) Experimentally determined external quantum efficiency (EQE) of the PV cell when equipped with the different ARCs or polymer (PMMA) coatings, and (d) their corresponding reflection spectra as measured experimentally.

Thus, through the selection of a material, whose refractive index closely aligns with the optimal 1.8–2.2 range identified in Figure 3b, the reflection losses can be largely suppressed. However, the optical materials utilized in an ARC must not only possess a suitable refractive index but also be highly transmissive across a broad range of wavelengths. This includes chemical, optical, and mechanical stability under the intense solar spectrum for prolonged periods of time, readily achievable adhesion to the Si substrate, little or no reactivity with other thin-film materials, and the absence of a tendency to crack under mechanical stress.⁵¹ Deposition of the AR material(s) should also be completely compatible with the state-of-the-art solar cell manufacturing and processing techniques. The materials selected and investigated in this study are fulfilling most, if not all, of these design requirements.

The magnitude of the reflection losses originating from the front surface of the PV device can be further alleviated through complementing the choice of design material(s) with the appropriate optical thickness (λ_0). Figure 3 emphasizes this ability of the fitted PV device to couple more effectively the

light into the mc-Si cell in response to an amending thickness of the single-layer ARC. Figure 3c confirms the notion that selecting the right material for the AR component can result in a substantial decrease in the spectral losses of the PV device. A decrease in the R_c value was observed from 0.35 for pristine (Figure 3c—dashed black line) to 0.15 ± 0.04 for ITO (Figure 3c—black circle) or to 0.17 ± 0.04 for TiO₂ (Figure 3c—cyan triangle). Consequently, this can lead, respectively, to a 68 to 43% enhancement in the electromagnetic radiation transmitted to the PV substrate (Figure 3c). Through the optimization of the film's thickness to act as a quarter-wavelength thick optical medium at 600–650 nm, this enhancement was pushed as high as 69% (ITO, Figure 3c). The controlled modification of the PV device's optical properties resulted in a 31% (ITO) to 55% (ZnO) increase in the J_{sc} generated within the photoconductive material, in comparison to the untreated pristine PV architecture (Figure 3d). The main limitation affecting single-layer ARC designs is their limited ability to offer reflection suppression only over a single and relatively narrow band of frequencies. To effectively target a much wider range

of frequencies within the solar spectrum and leverage the power of multiple different types of AR materials, the architecture of this simplistic design must be adapted to include more than one AR layer.

3.2. Model Validation. **3.2.1. Optical Properties.** The structures represented within the modeling environment were assumed to exhibit a complete uniformity of their optical properties (refractive index, optical thickness). The close agreement between the modeled and measured reflectance spectra shown in Figure 4 ensured the suitability of the TMM to effectively handle the more complex optical designs of the SE-devices.

3.2.2. Short-Circuit Current Density Component. Considering that the TMM in its generalized formalism cannot accurately describe the optical behavior of a structured/textured PV architecture,⁵² it was essential to find a suitable multilayered structure that could effectively imitate the spectral and electrical characteristics of this type of PV architecture. The ultralow reflectance (<2%) achieved with the most commercially mature textured/structured Si architecture is demonstrated in Figure 5a (mc-Si PV Cell) and shows almost complete suppression of the reflection losses over the 300–1100 nm range. Recreating this optical behavior in its entirety using only planar optical interfaces of differing refractive indices can be challenging but not impractical. The modeled PV architecture, which was used to emulate the optical behavior of the surface-textured mc-Si cell (Figure 5—modeled mc-Si PV cell), was composed of five distinct thin films, each of which was composed of idealized optical materials³⁵ whose refractive index and optical thickness were attuned to suppress reflections at a wavelength of 600 nm.³⁵ Starting from the Si substrate, the five layers considered in the model had the following refractive index n and thickness t : $n_1 = 3.09$, $t_1 = 49$ nm; $n_2 = 2.47$, $t_2 = 61$ nm; $n_3 = 1.97$, $t_3 = 76$ nm; $n_4 = 1.57$, $t_4 = 96$ nm; $n_5 = 1.25$, $t_5 = 120$ nm. Through utilizing this theoretical multilayered design, a reflectance spectrum approximately matching that of the commercial grade mc-Si cell was obtained (Figure 5, imitated PV cell—red triangles).⁷ However, a reflectance loss of 5–25% remained over the 300–450 nm range for the emulated architecture. Coincidentally, this narrow band of frequencies is within the spectral range where the luminophores are mainly absorbing (see Figure 1b.iii) and where the spectral response of mc-Si is relatively low (0.1–0.2 A W⁻¹). Consequently, the discrepancy between the “modeled” and the “real” PV devices’ reflectance spectra is expected to have very little influence over the performance metrics (R_e , J_{sc}), utilized to evaluate and optimize the collection efficiency of the newly proposed solar cell designs. This aspect is highlighted by the close agreement between the R_e of the two devices (modeled—PV cell and measured—mc-Si PV cell), as shown in the inset of Figure 5a. Through the subsequent fitting of single-layer transparent thin-films and polymeric encapsulants onto the modeled PV cell, the predicted electrical behavior of these modeled devices was effectively compared to their experimental counterparts.

The comparison between the electrical performances exhibited by the modeled devices and those fabricated and characterized experimentally is presented in Figure 5b. A small divergence between the expected (modeled) and real-world (experimental) performances of each iteration of the PV device can be observed. The discrepancy in the J_{sc} is ranging from -5.1 mA cm⁻² (Figure 5b—TiO₂) to $+3.5$ mA cm⁻² (Figure 5b—mc-Si PV Cell) for the modeled devices.

The differences between the behavior of the modeled and actual PV devices are expected, as the fundamental nature of the interactions of light with the highly ordered textured surface (shown in the inset of Figure 5b) are unaccounted for in the modeling environment. Additionally, the “class A” solar simulators for the AM1.5G spectrum (utilized to simulate the natural climate conditions in the modeling environment) can have tolerances of $\pm 25\%$ under the standardized testing guidelines.¹⁵ Consequently, the spectral mismatch between the spectral irradiance provided to the modeled and experimental devices could have influenced the resulting current densities generated. Furthermore, in the simplification of the calculations involved in modeling the PV devices, a number of additional loss pathways (including back surface reflection losses, band offsets, changes in the sheet and serial resistance, thermalization losses, and the possibility of “poor” electrical contact as a result of preparing the cells for indoor characterization) were excluded from the analysis. Consequently, by comparing the photocurrent generated within the modeled PV architecture (which includes contributions from the surface-textured ARC) with the current density delivered by an untreated silicon device, the increase in the collection efficiency stemming from the surface texturing can be determined. Thus, the integration of the surface-textured ARC (highlighted in the inset of Figure 5b) enhances the collection efficiency of the untreated silicon from 19.6 to 30.8 mA cm⁻² (Figure 5b—mc-Si PV cell).

However, it should be noted that this short-circuit current density does not include the reduction in efficiency that is expected to arise once an additional optical layer (either an encapsulant or an ARC) has been fitted directly on top of the already present textured coating. Indeed, when an additional optical structure (as those presented in Figure 5c) has been deposited on top of the textured mc-Si cell, a reduction in the number of charge carriers that was produced across the spectral response range of mc-Si was noted (see Figure 5c). This behavior is expected to stem from the disruption of the antireflection properties exhibited by the textured surface of the mc-Si cell. The magnitude of the deviations introduced into the external quantum efficiency (EQE) of the resulting PV devices was relatively small for the addition of the ARCs (0.02–0.05).

The incorporation of relatively thick PMMA encapsulant resulted in a significant deterioration (0.10–0.15) in the EQE across the entire 300–1100 nm range (Figure 5c). The origin of the reduction witnessed in the EQE is also likely to coincide with the distribution of the antireflective properties of the textured coating, and indeed, an abrupt change in the reflection spectrum upon the addition of the polymeric layer was observed (Figure 5d). The magnitude of the deviations introduced into the external quantum efficiency (EQE) of the resulting PV devices was relatively small for the addition of the ARCs (0.02–0.05). Consequently, the presence of a protective encapsulation layer for most commercial PV applications that are based upon the mc-Si architecture (like the one utilized in this study) can lead to a 10–15% reduction of charge carriers that are created across the response range of the PV material. This deterioration in the conversion performance of mc-Si can be significant considering that the typical thicknesses of the encapsulation employed in commercial mc-Si modules are orders of magnitude greater (e.g., ~ 5 –20 mm) than in the configurations explored in this study. This result demonstrates the need to reconsider the

design of the encapsulation materials that are conventionally employed in mc-Si modules to maximize the cooperative interactions that can arise between the different optical layers that protect and insulate the PV module from the environment.

Nevertheless, the data generated throughout this comparison were used to recalibrate the short-circuit current density generated in the subsequently modeled SE-device architectures. To ensure that the performance of the modeled SE-devices was in-line with a tangible improvement, a cautionary adjustment of -5.1 mA cm^{-2} (the most severe divergence reported in Figure 5b) was henceforth implemented in all of the calculations involved. The application of the correction factor enables the cumulative contribution of the loss mechanisms available in an experimental scenario (some of which are outlined above), to be included in the analysis without the requirement of knowing the extent of their individual contributions.

3.3. Structure-Enhanced Devices. **3.3.1. Structure-Enhanced LDS Devices.** In the pursuit of highly efficient LDS devices, many different configurations of optical thickness have been reported in the literature, with values ranging from $5 \mu\text{m}$ to 5 mm .^{2,3,15,60} Although none of the optical modes of interaction that can take place between a luminophore and the spectral irradiance were considered in the model, their potential to restrict the underlying enhancement mechanisms of the structure-enhanced designs proposed in this study was integrated in the design criterion. Typically, the interaction window of most luminescent materials utilized in LDS applications is confined to the $300\text{--}500 \text{ nm}$ spectral window, and consequently, the integration of ARCs designed to minimize the reflections occurring at 600 nm (Figure 3a) should not impede the functionality of the fluorescent compounds. Integrating a relatively thick PMMA layer can determine the appearance of interactions between the luminescent material embedded in the host polymer and the incoming radiation.⁷ However, in this scenario, the embedded luminophore(s) could be predisposed to aggregation processes, which can adversely affect the photoluminescent properties of the layer.^{7,53,54} Selecting a thinner PMMA layer allows for a reduction in the amount of luminescent material used, and additionally, it offers an increased control over the interactions between the embedded luminescent molecules.^{53–55} Therefore, using a thinner PMMA layer could offer more advantages of the design and could assist in mitigating the drawbacks of the optically thick LDS devices. Figure 6 presents the optical (R_e) and electrical (J_{sc}) performance of a PMMA-fitted mc-Si PV as the modeled thickness of the encapsulation is increased from 1 nm to $1 \mu\text{m}$ using the computational approach presented earlier.

It can be observed that as the thickness of the PMMA layer is varied from 1 to 150 nm , the polymeric layer behaves like an ARC. Thus, a reduction in the R_e (Figure 6—black squares) and enhancement in the photocurrent J_{sc} (Figure 6—blue circles) can be generated by the presence of the PMMA-device on top of the pristine PV. These results were anticipated as the presence of an additional thin-film coating of comparatively low refractive index ($n_{\text{PMMA}} \approx 1.5$) can expand the graded-index profile of the device. In turn, this leads to smaller light losses at each optical interface. At intermediate thicknesses of the PMMA layer (i.e., $0.150\text{--}0.500 \mu\text{m}$) the change in the PV performance is not as regular (Figure 6).

This variation in the PMMA layer optical behavior has its roots in the shift from environments suitable for the coherent

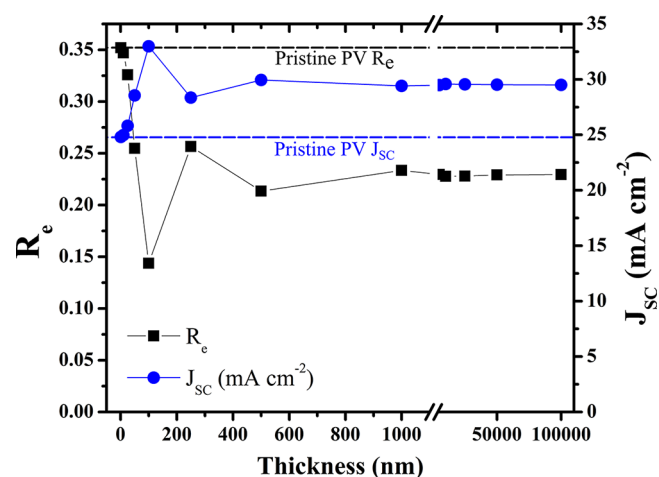


Figure 6. Effective weighted average reflectance (R_e) and short-circuit current density (J_{sc}) as influenced by the thickness of the pristine PMMA coating.

light propagation (analogous with thin-film interference) to circumstances that endorse the narrow-band oscillations in the reflectance and transmittance spectra.^{35,56} Such conditions are, typically, occurring when the polymeric encapsulation becomes much “thicker” than the wavelength of the electromagnetic radiation impinging the layer.^{35,56}

These oscillations, typically named “incoherent interference interactions”, are not often observed in practical measurements.⁵⁶ As the thickness of the PMMA is increasing, the fluctuations introduced by the presence of the SE-devices are attenuated (Figure 6). Enhancements of 35 and 20% were obtained in the R_e and J_{sc} , respectively, when a PMMA layer with a thickness between 1 and $100 \mu\text{m}$ was employed. Hence, two possible configurations of the PMMA layer were integrated into the modeling of the SE-designs to maximize the cooperative contribution brought by the constituent optical elements of the SE-devices: a relatively thick ($100 \mu\text{m}$, see Figure 7—green triangles) and thinner ($10 \mu\text{m}$, see Figure 7—orange circles) PMMA layer.

The pristine mc-Si cell has an R_e value of 0.35 (Figure 7a), which translates into an optical collection efficiency of 65% (Figure 7a). This implies that 65% of the impinging photons are available to generate charge carriers in the photoconductive material. This optical behavior translates into a J_{sc} of $\sim 19.6 \text{ mA cm}^{-2}$ in accordance with the spectral responsivity of the silicon architecture. Fitting a PMMA encapsulant on top of the PV cell leads to an additional 12% of the solar radiation being now available to create charge carriers. This suggests that, in comparison with the bare PV, the PMMA SE-device leads to a $33.1 \pm 0.4\%$ enhancement in the J_{sc} (Figure 7b—PMMA SE-device). It should be noted that this enhancement in the collection efficiency does not contain the photons emitted by the luminophore (or their plasmonic coupled equivalents), and it arises only from the optical matching of the materials. This suggests that, even in the absence of photoluminescence, an increase in the performance of the mc-Si cell can be achieved by encapsulating the structure in a PMMA film with an optical thickness of between 0.010 and 0.100 mm . Therefore, the enhancement could be even larger if the modulated solar spectrum contributions (arising through PLDS) will be also included, but such a study is not within the object of the present work.

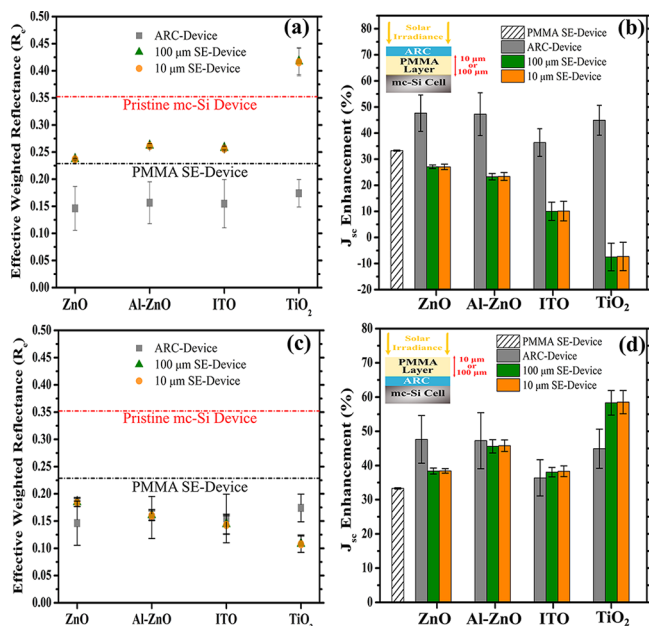


Figure 7. Enhanced effective weighted reflectance (R_e) (a,c) and the short-circuit current density (J_{sc}) (b,d) as foreseen to be achieved using two varieties of structure-enhanced (SE) layer designs (see insets for the schematics): structures incorporating a single-layer ARC (various materials being used) placed (1) above (a: R_e ; b: J_{sc}) or (2) the PMMA layer. Two different thicknesses (100 μm (green triangles) and 10 μm (orange circles)) of the PMMA layer were modeled in the initial designs. The error bars reflect the variability of the improvement introduced by the thickness. The materials order reflects the increase in the refractive index.

An increase in the reflection losses (Figure 7a) was observed when a single-layer ARC was placed directly above the polymeric encapsulation (inset of Figure 7b) into the SE-design. This increase in the reflection losses was seen independently of the material used for the ARC. This suggests that in this type of device configuration, where the transparent ARC material has a refractive index lower than $n_{\text{PMMA}} \approx 1.5$,^{57,58} the presence of the ARC disrupts the light interaction with the SE structure. Thus, a single-layer ARC inserted above the PMMA layer leads to a decrease in the harvested solar energy from $4.5 \pm 0.7\%$ (Figure 7b, ZnO) to $30 \pm 5.2\%$ (Figure 7b, TiO_2) when compared to the PMMA SE-device (Figure 7b, PMMA SE-device). This comportment of the single-layer ARC within the SE structure is most probably due to the effective refractive index of the retrofitted SE structure being larger than the refractive index of the mc-Si PV.³⁵ Therefore, the reflections occurring at the optical interfaces along the stratified SE-device lead to a decrease in the SE-device efficiency to collect the incoming solar energy, when compared to the unmodified PMMA SE-device.⁷ For thin films, the effective refractive index can be considered as resulting from the fact that a multilayered film (unlike a mixture of different materials) often works as a single homogeneous film, i.e., it exhibits an effective refractive index different from the individual refractive indexes of its constituents.^{7,35,56} When the condition $n_{\text{PMMA}} < n_{\text{ARC}} < n_{\text{Si}}$ is broken, the fixed-phase relationship (due to the optical interfaces within the stratified architecture) between the multiple reflections cannot sustain the occurrence of the destructive interference.^{35,56} Instead, both constructive and destructive interference are occurring. The constructive

interference leads to an increase in the losses at the front side of the device (Figure 7a). Therefore, when the graded step-down refractive index relationship (i.e., $(n_{\text{PMMA}} < n_{\text{ARC}} < n_{\text{Si}})$) of the SE-device is altered, the antireflective properties of the additional PMMA layer and ARC are canceled. This, in turn, will lead to a negative enhancement (i.e., a decrease) in the PV performance.

When the ARC is incorporated below the PMMA layer in the SE-device design (see the inset in Figure 7d), the graded step-down refractive index profile (i.e., $n_{\text{PMMA}} < n_{\text{ARC}} < n_{\text{Si}}$) of the device was preserved. Consequently, the presence of the ARC contributed to an additional increase, when compared to the PMMA SE-device, from 1% (Al-ZnO—Figure 7c) to 12% (TiO_2 —Figure 7c) in the spectral irradiance reaching the PV substrate. Besides these transmittance improvements, an increase of $3 \pm 0.9\%$ (ITO—Figure 7d) to $18.9 \pm 3.6\%$ (TiO_2 —Figure 7d) in the J_{sc} was observed, when compared to the standalone PMMA SE-device. Moreover, another improvement of 0.1 to 0.3% in the J_{sc} was obtained by decreasing the thickness of the polymeric encapsulation from 0.100 to 0.010 mm (Figure 7d). Furthermore, once the ARC thickness was optimized, this SE-device maintained a 2.5% (ITO—Figure 7d) to 13% (TiO_2) increase in the maximum J_{sc} that was delivered by the cell. Subsequently, the present results suggest that the collaborative interactions among the optical components (PMMA layer, Si substrate, and ARC) can be maximized leading to an enhanced collection efficiency that can be superior to that achieved with a classical LDS approach. To achieve this, however, a careful consideration should be given to the ARC composition and optical thickness of the layers in an SE-device.

4. CONCLUSIONS

A series of highly transparent antireflection coatings were investigated in order to be exploited in conjunction with the optical properties of conventional LDS and PLDS layers built upon a monocrystalline-silicon photovoltaic cell to enhance the energy conversion. The capability to tune the optical properties of the standalone single-layer antireflection coatings was theoretically explored (and experimentally tested) in response to changes in the effective refractive index and the optical thickness of the coating. The associated influence of each iteration of the supplementary optical structures on the conversion efficiency of the PV cell was investigated, and the optimal design criteria for this type of structure-enhanced (SE) device were identified. Through a combination of experimental and theoretical approaches, the reflectance spectra of the individual components of the SE-device (the PMMA layer, the Si substrate, and the thin-film (ARC) component) were accurately predicted within the modeling environment. Comparing the corresponding short-circuit current density generated within these modeled and experimental devices enabled the performance output of the model to be directly correlated and adjusted with the performances achieved under real-world laboratory conditions. As a result, the encapsulation of the pristine mc-Si PV device with a 10–100 μm thick PMMA coating predicted a $33.5 \pm 0.4\%$ increase in the collection efficiency, as inferred through the J_{sc} . This improved collection performance occurred even when only the PMMA layer was used in the modeled optical system. Hence, this can suggest that the energy harvesting potential of the system could potentially be further improved by the modulation of the solar irradiance, which can occur by inserting luminophores or

metal nanoparticles (i.e., via LDS or PLDS layers, respectively). Through the modeled integration of a single-layer ARC into the SE-device, an additional 2–22.5% enhancement in the predicted collection efficiency was achieved. Downsizing the PMMA layer from a thickness of 100 to 10 μm in the SE-device also assisted in promoting an additional 0.1–0.3% increase in the enhancement. Furthermore, the collection efficiency of the SE-device is predicted to outperform an ARC-fitted mc-Si cell by 2.5–13% when the ARC consists of the same optical materials. Consequently, through correspondingly fine-tuning the structural element in the SE-devices, the photocurrent generated within a conventional mc-Si cell is predicted to have a 6.7–11.4 mA cm^{-2} increase only through optical matching of the construction materials. The divergence in the optical response of the two SE-device designs envisioned facilitated the development and refinement of an initial set of design considerations for this type of architecture. Although the optical parameters of the ARCs employed in the SE-devices were optimized for an aluminum back-surface-field Si PV cell, the parameters (optical thickness and refractive index) can differ depending on the spectral responsivity of the underlying photovoltaic material upon which the device is constructed, but the method proposed in this study can be easily modified to be applied to any PV device.

■ ASSOCIATED CONTENT

SI Supporting Information

The Supporting Information is available free of charge at <https://pubs.acs.org/doi/10.1021/acsaelm.1c00018>.

The Supporting Information for this Article contains additional details on the validation of the theoretical model that was used to explore the different configurations of the structure-enhanced photovoltaic devices proposed herein. In section 1 of the Supporting Information, a complementary discussion of the complexities of accurately representing the series of optical materials that were used in the modeling environment to aid the investigation is presented. This includes a brief description of the construction material's refractive index and its origins in Figure S1, followed by an outline of the optical thickness of the structure-enhanced designs in Figure S2 that were considered during the model's validation process. In addition, the Supporting Information also includes complementary schematics of the photovoltaic samples produced (Figure S3—Section 2 of the Supporting Information) and the accompanying experimental setup (Figure S4—Section 3 of the Supporting Information) that were used to characterize their optical behavior (PDF)

■ AUTHOR INFORMATION

Corresponding Author

James Walshe – Dublin Energy Lab, Technological University Dublin, Dublin 8, Ireland; School of Physics & Clinical & Optometric Sciences, Technological University Dublin, Dublin D08 NF82, Ireland; orcid.org/0000-0001-9636-8990; Email: jameswalshe74@yahoo.ie

Authors

Mihaela Girtan – Photonics Laboratory, (LPhiA) E.A. 4464, SFR Matrix, Université d'Angers, 49000 Angers, France; orcid.org/0000-0002-8058-4143

Sarah McCormack – Department of Civil, Structural & Environmental Engineering, Trinity College Dublin, Dublin 2, Ireland

John Doran – Dublin Energy Lab, Technological University Dublin, Dublin 8, Ireland; School of Physics & Clinical & Optometric Sciences, Technological University Dublin, Dublin D08 NF82, Ireland

George Amarandei – School of Physics & Clinical & Optometric Sciences, Technological University Dublin, Dublin D08 NF82, Ireland

Complete contact information is available at: <https://pubs.acs.org/doi/10.1021/acsaelm.1c00018>

Author Contributions

The manuscript was written through contributions of all authors. All authors have given approval to the final version of the manuscript.

Notes

The authors declare no competing financial interest.

■ ACKNOWLEDGMENTS

The authors, James Walshe, John Doran, George Amarandei, and Mihalea Girtan, are thanking the Irish Research Council (IRC) and Campus France, respectively, for the funding support through the Ulysses programme: grant no: "Ulysses 4103SSM - Development and characterization of Bragg-type layers for efficiency enhancement of photovoltaic cells".

■ REFERENCES

- (1) Häberlin, H. Solar Modules and Solar Generators. *Photovoltaics: System Design and Practice* **2012**, 127–221.
- (2) De la Mora, M. B.; Amelines-Sarria, O.; Monroy, B. M.; Hernández-Pérez, C. D.; Lugo, J. E. Materials for Downconversion in Solar Cells: Perspectives and Challenges. *Sol. Energy Mater. Sol. Cells* **2017**, 165, 59–71.
- (3) McKenna, B.; Evans, R. C. Towards Efficient Spectral Converters through Materials Design for Luminescent Solar Devices. *Adv. Mater.* **2017**, 29 (28), 1606491.
- (4) Luceño-Sánchez, J. A.; Díez-Pascual, A. M.; Peña Capilla, R. Materials for Photovoltaics: State of Art and Recent Developments. *Int. J. Mol. Sci.* **2019**, 20 (4), 976.
- (5) Klampaftis, E.; Richards, B. S. Improvement in Multi-Crystalline Silicon Solar Cell Efficiency via Addition of Luminescent Material to EVA Encapsulation Layer. *Prog. Photovoltaics* **2011**, 19 (3), 345–351.
- (6) Gabr, A. M.; Walker, A. W.; Wilkins, M. M.; Kleiman, R.; Hinzler, K. Procedure to Decouple Reflectance and Down-Shifting Effects in Luminescent down-Shifting Enhanced Photovoltaics. *Opt. Express* **2017**, 25 (12), A530–A538.
- (7) Walshe, J.; Girtan, M.; McCormack, S.; Doran, J.; Amarandei, G. Exploring the Development of Nanocomposite Encapsulation Solutions for Enhancing the Efficiency of PV Systems Using Optical Modelling. *Opt. Mater.* **2021**, 111, 110654.
- (8) Chiromawa, N.; Ibrahim, K. Effects of Poly (Methyl Methacrylate) PMMA, Film Thickness in the Light Transmission through SiO₂ for Applications in Solar Cells Technology. *IJEIT* **2015**, 5 (1), 125–131.
- (9) Conibeer, G. J.; Willoughby, A., Eds. *Solar Cell Materials: Developing Technologies*; Wiley Series in Materials for Electronic & Optoelectronic Applications; Wiley, 2014.
- (10) Day, J.; Senthilarasu, S.; Mallick, T. K. Improving Spectral Modification for Applications in Solar Cells: A Review. *Renewable Energy* **2019**, 132, 186–205.
- (11) Fraunhofer Institute for Solar Energy Systems. *Photovoltaics Report*; 2019.

- (12) International Energy Agency. *World Energy Investment Analysis Report*; 2019.
- (13) Partain, L.; Hansen, R. T.; Hansen, S. F.; Bennett, D.; Newlands, A.; Fraas, L. M. "Swanson's Law" Plan to Mitigate Global Climate Change. *2016 IEEE 43rd Photovoltaic Specialists Conference (PVSC)* **2016**, 3335–3340.
- (14) Alonso-Alvarez, D.; Ross, D.; Klampaftis, E.; McIntosh, K. R.; Jia, S.; Storiz, P.; Stolz, T.; Richards, B. S. Luminescent Down-Shifting Experiment and Modelling with Multiple Photovoltaic Technologies. *Prog. Photovoltaics* **2015**, *23* (4), 479–497.
- (15) Klampaftis, E.; Ross, D.; McIntosh, K. R.; Richards, B. S. Enhancing the Performance of Solar Cells via Luminescent Down-Shifting of the Incident Spectrum: A Review. *Sol. Energy Mater. Sol. Cells* **2009**, *93* (8), 1182–1194.
- (16) Ho, W.-J.; Feng, S.-K.; Liu, J.-J.; Yang, Y.-C.; Ho, C.-H. Improving Photovoltaic Performance of Silicon Solar Cells Using a Combination of Plasmonic and Luminescent Downshifting Effects. *Appl. Surf. Sci.* **2018**, *439*, 868–875.
- (17) Meng, L.; Wu, X.-G.; Ma, S.; Shi, L.; Zhang, M.; Wang, L.; Chen, Y.; Chen, Q.; Zhong, H. Improving the Efficiency of Silicon Solar Cells Using in Situ Fabricated Perovskite Quantum Dots as Luminescence Downshifting Materials. *Nanophotonics* **2019**, *9* (1), 93–100.
- (18) Chandra, S.; Doran, J.; McCormack, S. J.; Kennedy, M.; Chatten, A. J. Enhanced Quantum Dot Emission for Luminescent Solar Concentrators Using Plasmonic Interaction. *Sol. Energy Mater. Sol. Cells* **2012**, *98*, 385–390.
- (19) Walshe, J. *Innovative Nanomaterial Approaches For Solar Energy Applications*. Ph.D. Dissertation, Technological University Dublin: Dublin, Ireland, 2020; pp 133–168.
- (20) Walshe, J.; Carron, P. M.; McLoughlin, C.; McCormack, S.; Doran, J.; Amaranidei, G. Nanofluid Development Using Silver Nanoparticles and Organic-Luminescent Molecules for Solar-Thermal and Hybrid Photovoltaic-Thermal Applications. *Nanomaterials* **2020**, *10* (6), 1201.
- (21) Geddes, C. D., Ed. *Surface Plasmon Enhanced, Coupled and Controlled Fluorescence*; Wiley, 2017.
- (22) Pei, Y.; Yao, F.; Ni, P.; Sun, X. Refractive Index of Silver Nanoparticles Dispersed in Polyvinyl Pyrrolidone Nanocomposite. *J. Mod. Opt.* **2010**, *57* (10), 872–875.
- (23) Alisha; Rozra, J.; Saini, I.; Sharma, A.; Sharma, P. Tuning of Optical Properties of PMMA by Incorporating Silver Nanoparticles. *AIP Conf. Proc.* **2011**, *1447* (1), 237–238.
- (24) Darman Singho, N.; Che Lah, N.; Johan, M.; Ahmad, R. Enhancement of the Refractive Index of Silver Nanoparticles in Poly (Methyl Methacrylate). *Int. J. Res. Eng. Technol.* **2012**, *1*, 231–234.
- (25) Goyal, A.; Rozra, J.; Saini, I.; Sharma, P.; Sharma, A. Refractive Index Tailoring of Poly(Methylmethacrylate) Thin Films by Embedding Silver Nanoparticles. *Adv. Mater. Res.* **2012**, *585*, 134–138.
- (26) Leyre, S.; Proost, K.; Cappelle, J.; Durinck, G.; Hofkens, J.; Deconinck, G.; Hanselaer, P. Experimental Validation of Adding-Doubling Modeling of Solar Cells Including Luminescent down-Shifting Layers. *J. Renewable Sustainable Energy* **2015**, *7* (4), 043130.
- (27) Lipovšek, B.; Solodovnyk, A.; Forberich, K.; Stern, E.; Brabec, C. J.; Krč, J.; Topič, M. Optical Model for Simulation and Optimization of Luminescent Down-Shifting Layers in Photovoltaics. *Energy Procedia* **2015**, *84*, 3–7.
- (28) Hosseini, Z.; Ghanbari, T. Designing an Efficient Graphene Quantum Dot-Filled Luminescent down Shifting Layer to Improve the Stability and Efficiency of Perovskite Solar Cells by Simple Optical Modeling. *RSC Adv.* **2018**, *8* (55), 31502–31509.
- (29) Kennedy, M.; McCormack, S. J.; Doran, J.; Norton, B. Improving the Optical Efficiency and Concentration of a Single-Plate Quantum Dot Solar Concentrator Using near Infra-Red Emitting Quantum Dots. *Sol. Energy* **2009**, *83* (7), 978–981.
- (30) Walshe, J.; McCormack, S. J.; Ahmed, H.; Doran, J. A Transfer Matrix Approach to Aid in the Design and Optimization of Hybrid Advanced Passive Structures for Enhancing Photovoltaic Efficiency. *ISES Sol. World Congr. 2017 - IEA SHC Int. Conf. Sol. Heat. Cool. Build. Ind.* **2017**, *Proc.* **2017**, 1297–1305.
- (31) Walshe, J.; Ahmed, H.; McCormack, S. J.; Doran, J. Bragg Enhanced Plasmonic Luminescent Downshifting for PV Devices. *EUPVSEC Conf. Proc.* **2016**, 256–259.
- (32) Spinelli, P.; Lenzmann, F.; Weeber, A.; Polman, A. Effect of EVA Encapsulation on Antireflection Properties of Mie Nanoscatterers for C-Si Solar Cells. *IEEE J. Photovoltaics* **2015**, *5* (2), 559–564.
- (33) Phillips, B. M.; Jiang, P. Chapter 12 - Biomimetic Antireflection Surfaces. *Engineered Biomimicry* **2013**, 305–331.
- (34) El-Bashir, S. M.; Yahia, I. S.; Al-Harbi, F.; Elburaih, H.; Al-Faifi, F.; Aldosari, N. A. Improving Photostability and Efficiency of Polymeric Luminescent Solar Concentrators by PMMA/MgO Nanohybrid Coatings. *Int. J. Green Energy* **2017**, *14* (3), 270–278.
- (35) Pedrotti, F. L.; Pedrotti, L. S. *Introduction to Optics*, 2nd ed.; Prentice Hall, 1992.
- (36) Gueymard, C. A.; Myers, D.; Emery, K. Proposed Reference Irradiance Spectra for Solar Energy Systems Testing. *Sol. Energy* **2002**, *73* (6), 443–467.
- (37) Guo, X.; Liu, Q.; Tian, H.; Li, B.; Zhou, H.; Li, C.; Hu, A.; He, X. Optimization of Broadband Omnidirectional Antireflection Coatings for Solar Cells. *J. Semicond.* **2019**, *40* (3), 032702.
- (38) Sinha, G.; Yadav, R. K. Optimization of Multilayer Antireflection Coating for Visible Spectrum on Silicon Substrate for Solar Cell Application. *J. Opt. Technol.* **2015**, *82* (12), 827–830.
- (39) Zhan, F.; Li, Z.; Shen, X.; He, H.; Zeng, J. Design Multilayer Antireflection Coatings for Terrestrial Solar Cells. *Sci. World J.* **2014**, *2014*, 265351.
- (40) Fleischer, K.; Arca, E.; Shvets, I. V. Improving Solar Cell Efficiency with Optically Optimised TCO Layers. *Sol. Energy Mater. Sol. Cells* **2012**, *101*, 262–269.
- (41) Zhao, J.; Green, M. A. Optimized Antireflection Coatings for High-Efficiency Silicon Solar Cells. *IEEE Trans. Electron Devices* **1991**, *38* (8), 1925–1934.
- (42) Shabat, M. M.; Ubeid, M. F. Antireflection Coating at Metamaterial Waveguide Structures for Solar Energy Applications. *Energy Procedia* **2014**, *50*, 314–321.
- (43) Shabat, M. M.; El-Amassi, D. M.; Schaadt, D. M. Design and Analysis of Multilayer Waveguides Containing Nanoparticles for Solar Cells. *Sol. Energy* **2016**, *137*, 409–412.
- (44) Aiken, D. J. High Performance Anti-Reflection Coatings for Broadband Multi-Junction Solar Cells. *Sol. Energy Mater. Sol. Cells* **2000**, *64* (4), 393–404.
- (45) Zighed, L.; Mahdjoub, A. Comparative Study Between Various Antireflective Coatings For Solar Cells Applications. *IOP Conf. Ser.: Mater. Sci. Eng.* **2010**, *13*, 012037.
- (46) Stapinski, T.; Swatowska, B. Amorphous Hydrogenated Silicon–Carbon as New Antireflective Coating for Solar Cells. *J. Non-Cryst. Solids* **2006**, *352* (9), 1406–1409.
- (47) Ahmed, H. a.; Walshe, J.; Kennedy, M.; Confrey, T.; Doran, J.; McCormack, S. J. Enhancement in Solar Cell Efficiency by Luminescent Down-Shifting Layers. *Adv. Energy Res.* **2013**, *1* (2), 117–126.
- (48) Ananda, W. External Quantum Efficiency Measurement of Solar Cell. *Int. Conf. QIR: Int. Symp. Elect. Comp. Eng.* **2017**, 450–456.
- (49) Agroui, K. Indoor and Outdoor Characterizations of Photovoltaic Module Based on Multicrystalline Solar Cells. *Energy Procedia* **2012**, *18*, 857–866.
- (50) Green, M. A.; Keevers, M. J. Optical Properties of Intrinsic Silicon at 300 K. *Prog. Photovoltaics* **1995**, *3* (3), 189–192.
- (51) Raut, H. K.; Ganesh, V. A.; Nair, A. S.; Ramakrishna, S. Anti-Reflective Coatings: A Critical, in-Depth Review. *Energy Environ. Sci.* **2011**, *4* (10), 3779.
- (52) Beck, W. *Modeling and Design of Mixed-Coherence Optical Stacks*; ARL-TR; Army Research Laboratory, 2012.
- (53) Bradley, M. S.; Tischler, J. R.; Bulović, V. Layer-by-Layer J-Aggregate Thin Films with a Peak Absorption Constant of 106 Cm⁻¹. *Adv. Mater.* **2005**, *17* (15), 1881–1886.

- (54) Zhang, L.; Cole, J. M. Dye Aggregation in Dye-Sensitized Solar Cells. *J. Mater. Chem. A* **2017**, *5* (37), 19541–19559.
- (55) Chandran, S.; Begam, N.; Padmanabhan, V.; Basu, J. K. Confinement Enhances Dispersion in Nanoparticle–Polymer Blend Films. *Nat. Commun.* **2014**, *5* (1), 3697.
- (56) Guldin, S. Optical Aspects of Thin Films and Interfaces. *Inorganic Nanoarchitectures by Organic Self-Assembly* **2013**, 19–32.
- (57) Xi, J.-Q.; Schubert, M. F.; Kim, J. K.; Schubert, E. F.; Chen, M.; Lin, S.-Y.; Liu, W.; Smart, J. A. Optical Thin-Film Materials with Low Refractive Index for Broadband Elimination of Fresnel Reflection. *Nat. Photonics* **2007**, *1* (3), 176–179.
- (58) Schubert, E. F.; Kim, J. K.; Xi, J. Q. Low-Refractive-Index Materials: A New Class of Optical Thin-Film Materials. *Phys. Status Solidi B* **2007**, *244*, 3002–3008.
- (59) Sathya, P.; Natarajan, R. Design and Optimization of Amorphous Based on Highly Efficient HIT Solar Cell. *Appl. Sol. Energy* **2018**, *54*, 77–84.
- (60) Perveen, A.; Deng, L.; Muravitskaya, A.; Yang, D.; Movsesyan, A.; Gaponenko, S.; Chang, S.; Zhong, H. Enhanced Emission of In-Situ Fabricated Perovskite-Polymer Composite Films on Gold Nanoparticle Substrates. *Opt. Mater. Express* **2020**, *10* (7), 1659–1674.
- (61) Chang, S.; Li, Q.; Xiao, X.; Wong, K. Y.; Chen, T. Enhancement of Low Energy Sunlight Harvesting in Dye-Sensitized Solar Cells Using Plasmonic Gold Nanorods. *Energy Environ. Sci.* **2012**, *5* (11), 9444–9448.